Solutions to the MiniBooNE Anomaly from New Physics in Charged Meson Decays

Bhaskar Dutta[,1] Doojin Kim[,1] Adrian Thompson,[1] Remington T. Thornton[,2] and Richard G. Van de Water[2]

[1]*Mitchell Institute for Fundamental Physics and Astronomy, Department of Physics and Astronomy,*
Texas A&M University, College Station, Texas 77845, USA
[2]*Los Alamos National Laboratory, Los Alamos, New Mexico 87545, USA*

We point out that production of new bosons by charged meson decays can greatly enhance the sensitivity of beam-focused accelerator-based experiments to new physics signals. This enhancement arises since the charged mesons are focused and their three-body decays do not suffer from helicity suppression in the same way as their usual two-body decays. As a realistic application, we attempt to explain the MiniBooNE low energy excess utilizing this overlooked mechanism, uniquely realizing dark-sector interpretations as plausible solutions to the excess. As proof of the principle, we consider two well-motivated classes of dark-sector models, models of vector-portal dark matter and models of long-lived (pseudo)scalar. We argue that the model parameter values to accommodate the excess are consistent with existing limits and that they can be tested at current and future accelerator-based neutrino experiments.

Introduction.—The MiniBooNE excess of electronlike events at 4.8σ [1–3] has been considered as one of the renowned phenomena indicative of the existence of new physics beyond the Standard Model (SM). Although a recent study claims that a careful estimate of systematics associated with major backgrounds would reduce the confidence level [4], the excess remains evident and requires a reasonable explanation. Furthermore, the recent MicroBooNE result [5] constrains the $\Delta \to N\gamma$ background more stringently, disfavoring the possibility of its ~ 3 times more enhanced branching ratio (BR) [3]. This observation advocates the need for new physics to explain the MiniBooNE e/γ-like excess and the MicroBooNE suggestive coherentlike scattering excess, both at low energies relative to the beam energy. Various new physics scenarios have been proposed to explain the anomaly. Among them, neutrino-based solutions [6–43] have received particular attention, as they also accommodate the observation that the MiniBooNE off-target mode does not show any appreciable excess [44]. This particularly challenges dark-sector interpretations including the scenario in which dark-matter production occurs dominantly from the decay of neutral mesons (e.g., π^0) together with kinetic mixing between the SM photon and a dark-sector U(1) gauge particle, as they would give rise to a corresponding excess in the off-target mode [44,45]. In addition, most of the

solutions, including the neutrino-based explanations, are potentially in conflict with null signal observations at other neutrino experiments including CHARM-II, MINERνA, and T2K [46,47].

In light of this situation, we point out that a hypothetical decay of charged mesons (e.g., $\pi^\pm$ and $K^\pm$) to a new mediator [vector or (pseudo)scalar] together with a $\ell\nu_\ell$ pair can provide a robust solution to the MiniBooNE anomaly that is nearly immune to the aforementioned issues, taking a few benchmark scenarios. In particular, we demonstrate that this class of explanations can render dark-sector interpretations (e.g., dark matter and long-lived mediators) plausible solutions without involving neutrino-sector physics. We also briefly discuss the implications of the recent result from MicroBooNE on these solutions. We further point out that ongoing and upcoming accelerator-based neutrino experiments can test some of them, confirming the MiniBooNE excess.

New physics from the $\pi^\pm/K^\pm$ decays.—The two-body decay process of charged pion or kaon, $\pi/K \to \ell\nu_\ell$ ($\ell = e$, μ), is highly suppressed unlike the naïve phase-space expectation, because the chiral nature of the decay products forces the angular momentum conservation to hold in limited phase space. However, once another decay product is added, the angular momentum conservation can be easily satisfied, allowing the process to fully exploit the decay phase space. As a consequence, a three-body decay involving (bosonic) mediator φ, $\pi/K \to \ell\nu_\ell\varphi$, shown in Fig. 1(a), can be sizable despite the additional phase-space suppression in the three-body process [48–53]. We further find that this decay width enhancement of the three-body decay processes is so significant that the three-body processes can overcome the phase-space suppression and
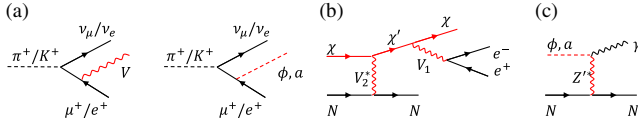
FIG. 1. (a) Three-body charged meson decay into a scalar, pseudoscalar, or vector. (b) Dark-matter upscattering via a vector mediator. In the single-mediator case, $V_2 = V_1$. (c) "Dark Primakoff" scattering of a scalar (ϕ)/pseudoscalar (a) via a Z'.

overwhelm the two-body processes with $\mathcal{O}(1)$ φ coupling. In particular, if φ is a massive vector, the corresponding enhancement becomes even more significant due to the existence of the longitudinal polarization mode [49,50]. Of course, $\mathcal{O}(1)$ φ coupling is unrealistic, as experimental measurements of the exotic decays of charged mesons set the upper limits of the BR of such decays to be $\sim 10^{-6} - 10^{-9}$ [54].

However, one can satisfy this upper limit with realistic coupling values allowed by existing bounds for new mediators such as scalar, pseudoscalar, and vector, and then expect a highly enhanced signal flux (either φ itself or φ-induced) responsible for the MiniBooNE excess. Moreover, signal loss could be minimized since most of the charged π/K's produced inside the MiniBooNE target are focused and directed to the MiniBooNE detector by the magnetic horn system before they decay. Therefore, this class of explanations can be consistent with the null signal observation in the off-target mode, as in the neutrino-based interpretations. We will attempt to explain the MiniBooNE excess using the $\pi^\pm/K^\pm$ signal; for proof of the principle, we consider benchmark *simplified* models of vector and (pseudo)scalar mediators containing only the particle contents relevant to explaining the MiniBooNE anomaly. We emphasize that the larger mass gap between K and the charged lepton opens more phase space than that in the π decay so that the K-induced contribution can be comparable to or even larger than the π-induced contribution despite its lower production rate, depending on the underlying model details.

Models.—(i) Vector-portal dark matter: Using the three-body decay modes of $\pi^\pm/K^\pm$, one can consider inelastic dark-matter models. For example, in a vector-portal dark-matter model, dark matter is produced by the decay of a dark-sector vector mediator (e.g., dark photon) and the scattering of the dark matter would contribute to the excess. The model is defined by the following interaction Lagrangian:

$$\mathcal{L}_V \supset \sum_{i=1,2} (e\epsilon_i J^\mu_{\text{EM}} + g_i J^\mu_D + g'_i J'^\mu_D) V_{i,\mu}, \quad (1)$$

where we generically assume the possibility that the vector mediator responsible for production of dark matter (say, V_1) can differ from the mediator appearing in the scattering process of dark matter (say, V_2) [55,56]. For illustration purposes, we assume that they are dark photons having

different mixing parameters, ϵ_1 and ϵ_2. J^μ_{EM} denotes the usual electromagnetic current in the SM, whereas J^μ_D and J'^μ_D describe the dark-sector currents involving only dark matter χ and involving dark matter and a heavier dark-sector state χ', correspondingly. To be fully general, we here separately introduce dark-sector couplings, $g_{1,2}$ and $g'_{1,2}$. Such models with detailed parameter-space analyses and UV completion were considered in the literature (e.g., Refs. [57–61]).

Once dark photon V_1 is created by the charged meson decays in the MiniBooNE target, it promptly decays to a χ pair. For illustration purposes, we assume that BR($V_1 \to 2\chi$) : $\sum_f$ BR($V_1 \to 2f$) = 50% : 50% with f running over all kinematically allowed SM fermions, and that mass relation $m_{V_1} < m_\chi + m_{\chi'}$ holds so that $V_1 \to \chi\chi'$ is kinematically forbidden. A produced χ reaches the MiniBooNE detector and scatters off either a nucleon or a carbon nucleus into the heavier state χ' via a t-channel exchange of V_1 (in the single-mediator scenario) or V_2 (in the double-mediator scenario). χ' then decays back to a χ and an (on-shell) V_1 which subsequently decays into an electron pair in the fiducial volume of the detector. Here, V_1 is significantly boosted, and therefore, the two Cherenkov rings induced by the electron pair typically overlap and appear single ring-like within the detector angular resolution or as small mass in a two ring fit [62]. We show this process in Fig. 1(b) and provide the scattering cross section formulas including the nucleon and nucleus form factors in literature (e.g., Refs. [63,64]). See Supplemental Material [65] and related references [55,56,59,63,66–68] for more details.

(ii) Long-lived (pseudo)scalar: In the next phenomenological model we consider a massive scalar ϕ or a massive pseudoscalar a that both couple to muons, and a massive vector mediator Z', with couplings to quarks as well as to the (pseudo)scalar through the CP-(odd)even operators, respectively. Explicitly, the interaction Lagrangians for these mediators are

$$\mathcal{L}_{S(P)} \supset g_n Z'_\alpha \bar{u} \gamma^\alpha u + \begin{cases} g_\mu \phi \bar{\mu} \mu + \frac{\lambda}{4} \phi F'_{\mu\nu} F^{\mu\nu} \\ i g_\mu a \bar{\mu} \gamma^5 \mu + \frac{\lambda}{4} a F'_{\mu\nu} \tilde{F}^{\mu\nu} \end{cases} + \text{H.c.}, \quad (2)$$

where g_μ, g_n, and λ parametrize coupling strengths for the operators and where $F'_{\mu\nu} \equiv \partial_\mu Z'_\nu - \partial_\nu Z'_\mu$ for Z' [69].

While the coupling to muons facilitates the production of ϕ or a from the charged mesons, similarly to the case of our vector portal model, in this situation we consider a long-lived ϕ or a that scatters inside the fiducial volume of the MiniBooNE detector via a Primakoff-like process shown in Fig. 1(c). Like the Primakoff scattering of neutral-pion or axionlike particle, this is a coherent process, but it instead takes place via the Z''s coupling to quark matter. This allows for a nuclear coherence, which we have parametrized by the Helm nuclear form factor [66].

In general, the long-lived (pseudo)scalar in Fig. 1(c) can be replaced by a long-lived vector mediator while a

(pseudo)scalar replaces the Z', and the related phenomenology in the context of the MiniBooNE excess is qualitatively and/or quantitatively similar to that of model (ii). Furthermore, depending on model details, one can envision the cases where the mediators in Fig. 1(a) can be attached to the $\pi^{\pm}/K^{\pm}/\nu$ legs as well as the $\ell^{\pm}$ leg.

Simulation.—Parametrizations of the charged meson fluxes at the MiniBooNE target are given in [78] for the Sanford-Wang (SW) and Feynman-Scaling (FS) approaches to modeling the $\pi^{\pm}$ and K^{+} fluxes, respectively. These parametrizations provide the double differential production cross sections of $\pi^{\pm}$ and K^{+} in the outgoing meson momentum p and angle θ with respect to the beam axis, as a function of the incident proton momentum. We have validated the SW and FS parametrizations by reproducing the MiniBooNE-modeled neutrino fluxes [78] to within an $\mathcal{O}(1)$ normalization difference. As the corresponding parametrization for K^{-} is unavailable, we instead adapt the FS-based Bonesini-Marchionni-Pietropaolo-Tabarelli model [79] to describe K^{-} production inside the target.

Most of the produced mesons enter the focusing-horn area where their momentum is (almost) aligned with the beam direction. The focusing-horn geometry allows mesons of $\theta \in (0.03, 0.21)$ radians to get focused [80]. We therefore select the mesons produced within this angular range out of the mesons simulated according to the above-described parametrizations and assume that their momentum becomes fully parallel to the beam axis by the focusing horn. We then check whether the chosen meson decays within 50 meters before reaching the dump area, using the usual decay law. The kinematics of the $\pi^{\pm}/K^{\pm}$ three-body decay, which involves production of mediator $\varphi(= V_1, a, \text{or } \phi)$, is taken care of by sampling the decay

events simulated with the MG5@aMC code package [81]. Hence, the total flux of mediator Φ_{φ} is

$$\Phi_{\varphi} = \sum_i \int_{\text{focus}} dE_i d\theta_i \frac{\partial^2 \Phi_i}{\partial E_i \partial \theta_i} \text{BR}(i \to \varphi), \qquad (3)$$

where i runs over all relevant mesons including the neutral and Φ_i denotes the flux of meson species i for a given protons-on-target (POT). Our Φ_i/POT are normalized to the corresponding numbers reported in [78].

In the dark-matter scenario, a produced V_1 promptly decays to a dark-matter pair by a 50% BR as mentioned earlier unless ϵ_1 is too small [82]. If a dark-matter particle passes through the detector fiducial volume, it can go through the process shown in Fig. 1(b). Therefore, the number of signal events N_S in the energy of the e^+e^- pair E_{ee} is

$$\frac{dN_S}{dE_{ee}} = 2\Phi_{V_1} \text{BR}(V_1 \to 2\chi) A_{\chi}^{\text{fid}} \frac{d\sigma_{\chi N}}{dE_{ee}} N_T^{\text{fid}} \text{BR}(V_1 \to 2e),$$

$$(4)$$

where A_{χ}^{fid}, $\sigma_{\chi N}$, and N_T^{fid} are the average probability that χ travels to the detector fiducial volume, the cross section of the $\chi N \to \chi' N$ scattering process, and the number of target nuclei or nucleons in the fiducial volume, respectively. Here, prefactor two accounts for the fact that V_1 decays to a dark-matter pair and Φ_{V_1} is given by Eq. (3) with φ replaced by V_1.

By contrast, in the pseudoscalar scenario [83], a produced a should reach the detector before it decays and undergo the scattering process shown in Fig. 1(c).
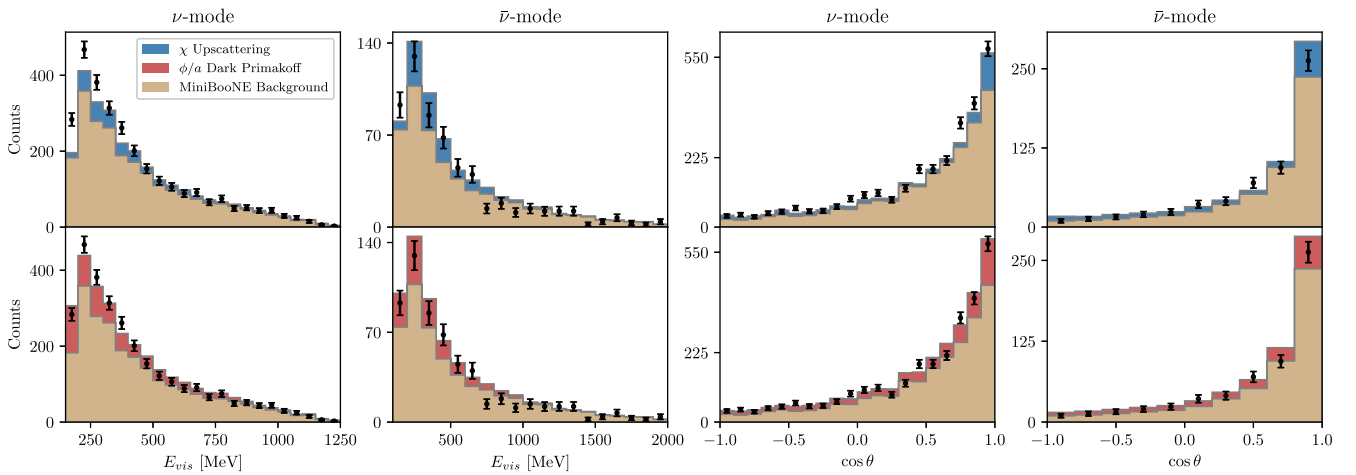

FIG. 2. Example fits for the vector-portal dark-matter scenario with double mediators (top panels) and the long-lived scalar scenario (bottom panels). The parameter values predicted by these fits and the associated χ^2 values are summarized in Table I. See the text for more detailed discussion.

TABLE I. Summary of example fits. In the single-mediator scenario, m_{V_2} is irrelevant, and $\epsilon_2 = \epsilon_1$ and $g_2' \to g_1'$. Because of the mass values of the mediators appearing in the scattering process, we fit the data in the limit of nucleon (nucleus) scattering for the double-mediator scenario (the others). The χ^2 in the parentheses are the values with statistics only.

Vector-portal dark matter			
Scenario	$(m_{V_1}, m_{V_2}, m_\chi, m_{\chi'})$	$\epsilon_1 \epsilon_2 g_2^2/(4\pi)$	χ^2/d.o.f.
Single	$(17, -, 8, 40)$ MeV	3.6×10^{-9}	2.5 (2.9)
Double	$(17, 200, 8, 50)$ MeV	1.3×10^{-7}	2.2 (2.6)

Long-lived (pseudo)scalar			
Scenario	$(m_{Z'}, m_{\phi/a})$	$g_\mu g_n \lambda$ (MeV^{-1})	χ^2/d.o.f.
Scalar	$(49, 1)$ MeV	2.2×10^{-8}	2.0 (2.1)
Pseudoscalar	$(85, 1)$ MeV	5.9×10^{-7}	2.0 (2.1)

The number of signal events as a function of the photon energy E_γ is then expressed as

$$\frac{dN_S}{dE_\gamma} = \Phi_a A_a^{\text{fid}} (1 - P_{\text{dec}}) \frac{d\sigma_{aN}}{dE_\gamma} N_T^{\text{fid}}, \qquad (5)$$

where A_a^{fid}, P_{dec}, and σ_{aN} denote the average probability that a travels to the detector fiducial volume, the average decay probability that a decays before reaching the detector, and the cross section of the $aN \to \gamma N$ scattering process. Again, Φ_a is given by Eq. (3) with φ replaced by a.

Fits and discussions.—We now reproduce the MiniBooNE excess (i.e., residual events) with respect to the two basic experimental observables, visible energy E_{vis} and the angle of visible particle(s) relative to the beam $\cos\theta$ in both neutrino and antineutrino modes, using our models described so far. The neutrino and antineutrino mode data are extracted from Ref. [3] and Ref. [2], respectively, and a 140 MeV energy threshold, a $< 10°$ angular separation for $e^+ e^-$ pairs, and energy-dependent detection efficiencies [84,85] are adopted. We then use the usual χ^2 function to estimate the goodness of the fit with statistical and systematic uncertainties added by quadrature. Here, we approximate systematics in backgrounds, based on the estimates in Table I in [3].

Example fits for models (i) and (ii) are displayed in the top panels and the bottom panels of Fig. 2, respectively, and the parameter and χ^2 values associated with these fits are summarized in Table I. The vertical bars describe the statistical uncertainties. For model (i) we assume fermionic χ, χ' and two different vector mediators V_1 and V_2, and for model (ii) we consider the scalar scenario. We also find reasonable fits for the long-lived pseudoscalar model as shown in Table I. Since MiniBooNE is sensitive to the product of the couplings involved in the scattering process in the detector and the coupling appearing in the charged
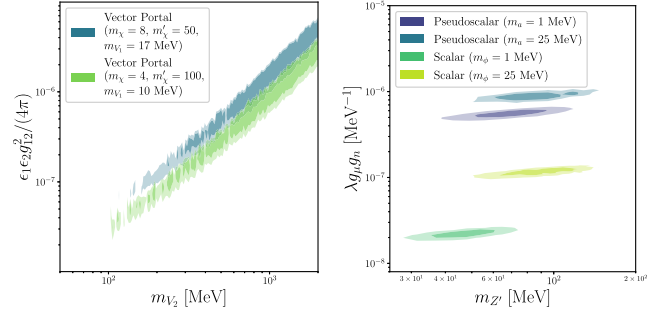

FIG. 3. The credible regions for fits to the MiniBooNE excess with model I (left) and model II (right) are shown at 68% (dark shaded) and 95% (light shaded).

meson decay, we report the product of those couplings. We emphasize that our goal here is to show that there exist a wide range of reasonable parameter sets (see, for example, Fig. 3), not to spot the best parameter point.

We next check if the parameter values for our fits satisfy existing bounds. First, since our mediators are from the charged-meson decay, the resulting decay widths should agree with exotic $\pi^\pm/K^\pm$ decays [54]. The relevant channels, limits, and BR predictions are summarized in Table II [86].

Second, the parameter points should not give rise to any significant number of events in the MiniBooNE off-target mode. Recall that our signal flux mostly originates from charged mesons that are focused, whereas that from neutral mesons are subdominant. In the off-target mode, $\sim$16 times smaller POTs were delivered, focusing was unavailable, and the π/K-decay-in-flight fluxes are smaller by $\sim$2 orders of magnitude [45]. Our off-target mode simulation suggests a negligible signal flux from charged mesons. In the single (double)-mediator scenario of model (i), we find that the conventional π^0 contribution consists of $\sim$4(8)% of signal, potentially yielding $\sim$2.4 $\pm$ 0.5 (4.4 $\pm$ 0.9) events in the off-target mode. This agrees with the data within the measurement uncertainty, or could be mitigated by an introduction of a vector mediator without any significant coupling to the first generation of quarks. For the (pseudo) scalar scenario, we find that $\sim$1 event is expected in the off-target mode.

Third, we check limits from other dark-sector particle search experiments. Since we assume that the dark photon(s) in model (i) are half-(in)visible, the limits of both invisibly and visibly decaying dark photons are relevant modulo the BR. For the parameter points in Table I, the leading limits are $\epsilon \approx 0.074(1.2) \times 10^{-3}$ for a 17 (200) MeV dark photon from NA64 (invisible dark photon decay) [89] and $\epsilon \approx 0.092(1.4) \times 10^{-3}$ for a 17 (200) MeV dark photon from E141 [90] and *BABAR* (visible dark photon decay) [91], which are reinterpreted again under the assumption that the BRs of the visibly and invisibly decaying modes are 50% and 50%. Our parameter choices mentioned in Table II are not excluded by these

TABLE II. Relevant exotic decays of $\pi^{\pm}/K^{\pm}$ and existing upper limits at 90% confidence level X stands for invisibly decaying (massive) bosons. The predicted BRs (third though last columns) are based on the following parameter choices: $[\epsilon_1, (g_1^2/4\pi)] \simeq (6.0 \times 10^{-5}, 1)$ for the single-mediator scenario, $[\epsilon_1, \epsilon_2, (g_2^2/4\pi)] \simeq (7.0 \times 10^{-5}, 1.0 \times 10^{-4}, 0.5)$ for the double-mediator scenario, $(g_\mu, g_n, \lambda) \simeq (5 \times 10^{-3}, 10^{-2}, 4.4 \times 10^{-4}\ \text{MeV}^{-1})$ for the scalar scenario, and $(g_\mu, g_n, \lambda) \simeq (10^{-2}, 10^{-2}, 6.5 \times 10^{-3}\ \text{MeV}^{-1})$ for the pseudoscalar scenario.

Channel (BR)	Limit ($\times 10^{-8}$)	Model (i) ($\times 10^{-12}$)		Model (ii) ($\times 10^{-8}$)	
		Single	Double	ϕ	a
$K \to \mu\nu_\mu V(\phi)$ [87]	2000 (300)	500	680	230	100
$K \to e\nu_e \nu\nu$ [54]	6000	530	720	$\cdots$	$\cdots$
$K \to \mu(e)\nu_{\mu(e)}ee$ [54]	7.4(2.7)	500(530)	680(720)	$\cdots$	$\cdots$
$\pi \to \mu(e)\nu_{\mu(e)}X$ [88]	600(50)	0.12(25)	0.17(34)	120($\cdots$)	1.1($\cdots$)
$\pi \to \mu(e)\nu_{\mu(e)}ee$ [54]	$-$(0.37)	0.12(25)	0.17(34)	$\cdots$	$\cdots$

experiments. Regarding the recent COHERENT result [92], we find that it is insensitive to our vector-portal dark-matter model. COHERENT would observe signal events through the coherent elastic scattering of our dark matter. However, as mentioned earlier, coupling g_1 is roughly proportional to ϵ_1 for our dark photon to be half-(in)visible, and thus the resulting scattering cross section at detection would be too small [93]. Regarding model (ii), we emphasize that the limits from other search experiments are highly model dependent, while we have not resorted to a particular model. For interested readers, we provide model examples accommodating (2) and useful references [94–96] in Supplemental Material [65] and explain how the related limits are evaded. A detailed study of UV models will be presented in an upcoming publication.

Fourth, we find that our models are consistent with the recent MicroBooNE results [5]. Compared to MiniBooNE, it is based on ∼3 times smaller POT [3,5], ∼6 times smaller fiducial volume [3,97], and ∼3 times smaller photon detection efficiency [5,85]. For a coherent scattering process the liquid argon of MicroBooNE gets a ∼3 factor increase relative to the mineral oil of MiniBooNE. This gives a net reduction factor of ∼18. Given that MiniBooNE observed 320 excess events below 300 MeV visible energy [3], then the models presented here with coherent scattering predict MicroBooNE would expect ∼18 event excess in the $1\gamma0p$ analysis at low energy. It is interesting that they report a 18 event (2.7σ) excess for the $1\gamma0p$ sample in the 200–250 MeV visible energy bin [5], demonstrating consistency with our predictions. Furthermore, the more recent MicroBooNE result demonstrates that less than approximately 50% of the MiniBooNE excess can come from ν_e charged-current scattering [98], suggesting that the majority of the excess is not from intrinsic ν_e backgrounds or sterile neutrino oscillations. This further bolsters the building evidence that the MiniBooNE excess is real and unexplained and it is potentially from a new source, such as the models presented here.

We finally remark that in the scalar and pseudoscalar scenarios, couplings such as $aF\tilde{F}$ are negligible in the fit to ensure decays $a \to \gamma\gamma$ do not contribute too much to the

forward events that would create too much of an excess in the forwardmost cosine bin.

Prospects at neutrino experiments.—Experiments that utilize proton beams and the induced neutrino fluxes should also be sensitive to new physics emerging in the charged mesons that we have used to explain the MiniBooNE excess [99]. Obviously, the experiments (e.g., SBND) using the same beam as for MiniBooNE can allow for checking the idea and predictions presented here [101]. Those using a higher-energy beam (e.g., DUNE/FASER/ICARUS-NuMI) can also test the proposed models, based on similar signal production mechanisms and detection channels. In particular, since charged mesons are produced with a larger boost, their decay products are more likely to lie in the forward region and thus a more signal flux can enter the detector [102].

Likewise, the low-energy high-intensity beam-based experiments (e.g., CCM/COHERENT/JSNS²) may have interesting opportunities. In these experiments, no beam focusing is available, so contributions from the charged mesons would be weakened, whereas those from the neutral mesons (e.g., π^0) would relatively stand out. Nevertheless, higher beam intensity and close proximity of the detector to the beam target would allow for a rather significant number of signal events. Especially, only the scattering-based MiniBooNE solutions involving $\mathcal{O}(1 - 10)$ MeV mediators can be directly checked in these experiments. In the case of model (i), signal detection via the dark-matter upscattering would not be available, as the associated dark-matter particles are not energetic enough to create a heavier state χ'. By contrast, given lower energy thresholds, coherent dark-matter elastic scattering can be promising for testing our dark-matter model in the double-mediator scenario, as g_2 can be sizable enough (unlike g_1) for ongoing/upcoming beam-based CEνNS experiments to observe signal events. On the other hand, in the case of model (ii), Z' can arise from the π^0 decay and decay into a (pseudo)scalar through $aF'\tilde{F}$ or $\phi F'F$. For signal detection, the same strategy is applicable. Again, thanks to the lower energy thresholds, both the outgoing photon and the nuclear recoil can be recorded simultaneously (i.e., fully visible), allowing us to infer

properties (e.g., mass) of the incoming particle more accurately. Finally, we remark that JSNS^2 can provide a unique opportunity especially if the MiniBooNE signal is only or dominantly sourced by charged kaons.

[1] A. A. Aguilar-Arevalo *et al.* (MiniBooNE Collaboration), Phys. Rev. Lett. **102**, 101802 (2009).

[2] A. A. Aguilar-Arevalo *et al.* (MiniBooNE Collaboration), Phys. Rev. Lett. **121**, 221801 (2018).

[3] A. A. Aguilar-Arevalo, B. C. Brown, J. M. Conrad, R. Dharmapalan, A. Diaz *et al.* (MiniBooNE Collaboration), Phys. Rev. D **103**, 052002 (2021).

[4] V. Brdar and J. Kopp, Phys. Rev. D **105**, 115024 (2022).

[5] P. Abratenko *et al.* (MicroBooNE Collaboration), Phys. Rev. Lett. **128**, 111801 (2022).

[6] M. Sorel, J. M. Conrad, and M. H. Shaevitz, Phys. Rev. D **70**, 073004 (2004).

[7] G. Karagiorgi, Z. Djurcic, J. M. Conrad, M. H. Shaevitz, and M. Sorel, Phys. Rev. D **80**, 073001 (2009); **81**, 039902(E) (2010).

[8] G. H. Collin, C. A. Argüelles, J. M. Conrad, and M. H. Shaevitz, Phys. Rev. Lett. **117**, 221801 (2016).

[9] C. Giunti and M. Laveder, Phys. Rev. D **84**, 073008 (2011).

[10] C. Giunti and M. Laveder, Phys. Lett. B **706**, 200 (2011).

[11] S. Gariazzo, C. Giunti, M. Laveder, and Y. F. Li, J. High Energy Phys. 06 (2017) 135.

[12] S. Böser, C. Buck, C. Giunti, J. Lesgourgues, L. Ludhova, S. Mertens, A. Schukraft, and M. Wurm, Prog. Part. Nucl. Phys. **111**, 103736 (2020).

[13] J. Kopp, M. Maltoni, and T. Schwetz, Phys. Rev. Lett. **107**, 091801 (2011).

[14] J. Kopp, P. A. N. Machado, M. Maltoni, and T. Schwetz, J. High Energy Phys. 05 (2013) 050.

[15] M. Dentler, A. Hernández-Cabezudo, J. Kopp, P. A. N. Machado, M. Maltoni, I. Martinez-Soler, and T. Schwetz, J. High Energy Phys. 08 (2018) 010.

[16] K. N. Abazajian *et al.*, arXiv:1204.5379.

[17] J. M. Conrad, C. M. Ignarra, G. Karagiorgi, M. H. Shaevitz, and J. Spitz, Adv. High Energy Phys. **2013**, 163897 (2013).

[18] A. Diaz, C. A. Argüelles, G. H. Collin, J. M. Conrad, and M. H. Shaevitz, Phys. Rep. **884**, 1 (2020).

[19] J. Asaadi, E. Church, R. Guenette, B. J. P. Jones, and A. M. Szelc, Phys. Rev. D **97**, 075021 (2018).

[20] G. Karagiorgi, M. H. Shaevitz, and J. M. Conrad, arXiv:1202.1024.

[21] H. Pas, S. Pakvasa, and T. J. Weiler, Phys. Rev. D **72**, 095017 (2005).

[22] D. Döring, H. Päs, P. Sicking, and T. J. Weiler, Eur. Phys. J. C **80**, 1202 (2020).

[23] V. A. Kostelecky and M. Mewes, Phys. Rev. D **69**, 016005 (2004).

[24] T. Katori, V. A. Kostelecky, and R. Tayloe, Phys. Rev. D **74**, 105009 (2006).

[25] J. S. Diaz and V. A. Kostelecky, Phys. Lett. B **700**, 25 (2011).

[26] J. S. Diaz and V. A. Kostelecky, Phys. Rev. D **85**, 016013 (2012).

[27] S. N. Gninenko, Phys. Rev. Lett. **103**, 241802 (2009).

[28] S. N. Gninenko and D. S. Gorbunov, Phys. Rev. D **81**, 075013 (2010).

[29] Y. Bai, R. Lu, S. Lu, J. Salvado, and B. A. Stefanek, Phys. Rev. D **93**, 073004 (2016).

[30] Z. Moss, M. H. Moulai, C. A. Argüelles, and J. M. Conrad, Phys. Rev. D **97**, 055017 (2018).

[31] E. Bertuzzo, S. Jana, P. A. N. Machado, and R. Zukanovich Funchal, Phys. Rev. Lett. **121**, 241801 (2018).

[32] P. Ballett, S. Pascoli, and M. Ross-Lonergan, Phys. Rev. D **99**, 071701(R) (2019).

[33] O. Fischer, A. Hernández-Cabezudo, and T. Schwetz, Phys. Rev. D **101**, 075045 (2020).

[34] M. H. Moulai, C. A. Argüelles, G. H. Collin, J. M. Conrad, A. Diaz, and M. H. Shaevitz, Phys. Rev. D **101**, 055020 (2020).

[35] M. Dentler, I. Esteban, J. Kopp, and P. Machado, Phys. Rev. D **101**, 115013 (2020).

[36] A. de Gouvêa, O. L. G. Peres, S. Prakash, and G. V. Stenico, J. High Energy Phys. 07 (2020) 141.

[37] A. Datta, S. Kamali, and D. Marfatia, Phys. Lett. B **807**, 135579 (2020).

[38] B. Dutta, S. Ghosh, and T. Li, Phys. Rev. D **102**, 055017 (2020).

[39] W. Abdallah, R. Gandhi, and S. Roy, J. High Energy Phys. 12 (2020) 188.

[40] A. Abdullahi, M. Hostert, and S. Pascoli, Phys. Lett. B **820**, 136531 (2021).

[41] J. Liao and D. Marfatia, Phys. Rev. Lett. **117**, 071802 (2016).

[42] M. Carena, Y.-Y. Li, C. S. Machado, P. A. N. Machado, and C. E. M. Wagner, Phys. Rev. D **96**, 095014 (2017).

[43] W. Abdallah, R. Gandhi, and S. Roy, Phys. Rev. D **104**, 055028 (2021).

[44] A. A. Aguilar-Arevalo, M. Backfish, A. Bashyal, B. Batell, B. C. Brown *et al.* (MiniBooNE DM Collaboration), Phys. Rev. D **98**, 112004 (2018).

[45] J. R. Jordan, Y. Kahn, G. Krnjaic, M. Moschella, and J. Spitz, Phys. Rev. Lett. **122**, 081801 (2019).

[46] C. A. Argüelles, M. Hostert, and Y.-D. Tsai, Phys. Rev. Lett. **123**, 261801 (2019).

[47] V. Brdar, O. Fischer, and A. Y. Smirnov, Phys. Rev. D **103**, 075008 (2021).

[48] V. Barger, C.-W. Chiang, W.-Y. Keung, and D. Marfatia, Phys. Rev. Lett. **108**, 081802 (2012).

[49] C. E. Carlson and B. C. Rislow, Phys. Rev. D **86**, 035013 (2012).

[50] R. Laha, B. Dasgupta, and J. F. Beacom, Phys. Rev. D **89**, 093025 (2014).

[51] P. Bakhti and Y. Farzan, Phys. Rev. D **95**, 095008 (2017).

[52] W. Altmannshofer, S. Gori, and D. J. Robinson, Phys. Rev. D **101**, 075002 (2020).

[53] G. Krnjaic, G. Marques-Tavares, D. Redigolo, and K. Tobioka, Phys. Rev. Lett. **124**, 041802 (2020).

[54] P. A. Zyla et al. (Particle Data Group), Prog. Theor. Exp. Phys. **2020**, 083C01 (2020).

[55] B. Dutta, D. Kim, S. Liao, J.-C. Park, S. Shin, and L. E. Strigari, Phys. Rev. Lett. **124**, 121802 (2020).

[56] B. Dutta, D. Kim, S. Liao, J.-C. Park, S. Shin, L. E. Strigari, and A. Thompson, J. High Energy Phys. 01 (2022) 144.

[57] D. Smith and N. Weiner, Phys. Rev. D **64**, 043502 (2001).

[58] E. Izaguirre, G. Krnjaic, P. Schuster, and N. Toro, Phys. Rev. D **90**, 014052 (2014).

[59] G. F. Giudice, D. Kim, J.-C. Park, and S. Shin, Phys. Lett. B **780**, 543 (2018).

[60] B. Dutta, S. Ghosh, and J. Kumar, Phys. Rev. D **100**, 075028 (2019).

[61] B. Dutta, S. Ghosh, and J. Kumar, Phys. Rev. D **102**, 075041 (2020).

[62] Another route of obtaining a single electronlike signature is highly energy-asymmetric e^+e^- pairs [32] in the three-body decay of χ' through an off-shell V_1.

[63] D. Kim, J.-C. Park, and S. Shin, Phys. Rev. Lett. **119**, 161801 (2017).

[64] D. Kim, P. A. N. Machado, J.-C. Park, and S. Shin, J. High Energy Phys. 07 (2020) 057.

[65] See Supplemental Material at http://link.aps.org/supplemental/10.1103/PhysRevLett.129.111803 for calculational details.

[66] R. H. Helm, Phys. Rev. **104**, 1466 (1956).

[67] I. A. Qattan et al., Phys. Rev. Lett. **94**, 142301 (2005).

[68] E. Borie, arXiv:1207.6651.

[69] These new bosons could appear, for example, in models with an extra gauged $U(1)_X$ symmetry and theories containing mixings between axionlike particles and dark photons (e.g., [70–77]).

[70] K. Kaneta, H.-S. Lee, and S. Yun, Phys. Rev. Lett. **118**, 101802 (2017).

[71] K. Kaneta, H.-S. Lee, and S. Yun, Phys. Rev. D **95**, 115032 (2017).

[72] A. Hook, G. Marques-Tavares, and C. Ristow, J. High Energy Phys. 06 (2021) 167.

[73] P. deNiverville, H.-S. Lee, and M.-S. Seo, Phys. Rev. D **98**, 115011 (2018).

[74] K. Choi, S. Lee, H. Seong, and S. Yun, Phys. Rev. D **101**, 043007 (2020).

[75] S. Biswas, A. Chatterjee, E. Gabrielli, and B. Mele, Phys. Rev. D **100**, 115040 (2019).

[76] O. E. Kalashev, A. Kusenko, and E. Vitagliano, Phys. Rev. D **99**, 023002 (2019).

[77] P. Arias, A. Arza, J. Jaeckel, and D. Vargas-Arancibia, J. Cosmol. Astropart. Phys. 05 (2021) 070.

[78] A. A. Aguilar-Arevalo et al. (MiniBooNE Collaboration), Phys. Rev. D **79**, 072002 (2009).

[79] M. Bonesini, A. Marchionni, F. Pietropaolo, and T. Tabarelli de Fatis, Eur. Phys. J. C **20**, 13 (2001).

[80] D. W. Schmitz, A measurement of hadron production cross sections for the simulation of accelerator neutrino beams and a search for ν_μ to ν_e oscillations in the δm^2 about equals $1 - eV^2$ region, Ph.D. thesis, Columbia University, 2008.

[81] J. Alwall, R. Frederix, S. Frixione, V. Hirschi, F. Maltoni, O. Mattelaer, H. S. Shao, T. Stelzer, P. Torrielli, and M. Zaro, J. High Energy Phys. 07 (2014) 079.

[82] Note that g_1 governing the $V_1 \to \chi\chi$ process is not a free parameter but determined by our BR assumption.

[83] For the scalar scenario, the corresponding formalism straightforwardly goes through with a replaced by ϕ.

[84] R. B. Patterson, E. M. Laird, Y. Liu, P. D. Meyers, I. Stancu, and H. A. Tanaka, Nucl. Instrum. Methods Phys. Res., Sect. A **608**, 206 (2009).

[85] E. Wang, L. Alvarez-Ruso, and J. Nieves, Phys. Lett. B **740**, 16 (2015).

[86] Be aware that the limits of the $K \to \mu\nu_\mu V(\phi)$ channel are available from 10 MeV, while our (pseudo)scalar has a 1 MeV mass.

[87] E. Cortina Gil et al. (NA62 Collaboration), Phys. Lett. B **816**, 136259 (2021).

[88] A. Aguilar-Arevalo, M. Aoki, M. Blecher, D. I. Britton, D. vomBruch et al. (PIENU Collaboration), Phys. Rev. D **103**, 052006 (2021).

[89] D. Banerjee et al., Phys. Rev. Lett. **123**, 121801 (2019).

[90] E. M. Riordan, M. W. Krasny, K. Lang, P. deBarbaro, A. Bodek et al., Phys. Rev. Lett. **59**, 755 (1987).

[91] J. P. Lees et al. (BaBar Collaboration), Phys. Rev. Lett. **113**, 201801 (2014).

[92] D. Akimov et al. (COHERENT Collaboration), First Probe of Sub-GeV Dark Matter Beyond the Cosmological Expectation with the COHERENT CsI Detector at the SNS, arXiv:2110.11453.

[93] By contrast, in COHERENT, α_D associated with g_1 is assumed to be 0.5.

[94] J. J. de Swart, M. C. M. Rentmeester, and R. G. E. Timmermans, PiN Newslett. **13**, 96 (1997).

[95] I. Holst, D. Hooper, and G. Krnjaic, Phys. Rev. Lett. **128**, 141802 (2022).

[96] B. Dutta, S. Ghosh, P. Huang, and J. Kumar, Phys. Rev. D **105**, 015011 (2022).

[97] P. Abratenko et al. (MicroBooNE Collaboration), Phys. Rev. D **104**, 052002 (2021).

[98] P. Abratenko et al. (MicroBooNE Collaboration), Phys. Rev. Lett. **128**, 241801 (2022).

[99] The long-lived (pseudo)scalar model can potentially explain the LSND excess [100] by initiating a neutron ejection from the inelastic interaction of Z' with a nucleus at the detector and subsequent neutron capture would produce the 2.2 MeV photon signal. However, since the proton beam energy of LSND is just 800 MeV, dark matter χ in model (i) would not upscatter to χ' that can create an electronlike signature through its decay, and thus the excess would not be explained.

[100] A. Aguilar-Arevalo, L. B. Auerbach, R. L. Burman, D. O. Caldwell, E. D. Church et al. (LSND Collaboration), Phys. Rev. D **64**, 112007 (2001).

[101] B. Dutta, D. Kim, A. Thompson, R. Thornton, and R. Van de Water (to be published).

[102] By contrast, this excess is not observable at CHARM-II, MINERνA, and T2K after considering their detector sizes, $\pi^\pm$ production rates, and target-to-detector distances altogether.